RUPTURE PREDICTION FOR SPACECRAFT PRESSURIZED TITANIUM TANKS

Robin Putzar*(1), Thomas Zweigle(1), Pascal Matura(1), Frank Bagusat(1), Markus Jung(1), Lukas Weninger(2), Tomas Garaj(2), Lukas Webinger(2), Mathias Redl(2), and Martin Schimmerohn(1)

(1)*Fraunhofer Institute for High-Speed Dynamics, Ernst-Mach-Institut, Ernst-Zermelo-Str. 4, 79104 Freiburg, Germany*
(2)*PEAK Technology GmbH, Technologiepark Str. 6, 4615 Holzhausen, Austria*

ABSTRACT

In ESA's "Impact-Safe Tank Pressure Level" ("ImSafT") study, tank rupture caused by hypervelocity impacts is investigated by both numerical simulations and hypervelocity impact experiments. The approach of the study is to verify the numerical simulations through available impact test data, use the so-verified models to predict critical impact conditions, confirm the predictions by experiments on sub-scale tanks, and finally perform full-scale simulations on realistic tank sizes. The major challenges for numerical simulations are the high strain rate impact loading of the tank wall material and large tank volumes in combination with comparatively thin tank walls. On the experimental side, the possible amount of impact tests is strongly limited by comparatively high manufacturing costs for realistic tank specimen. The experiments presented are currently being utilized in the still ongoing numerical parametric study.

1. INTRODUCTION

The majority of the current space debris population stems from fragmented satellites and rocket upper stages in orbit [7]. Pressure vessels and fuel tanks of space propulsion systems have a particular role in such explosion scenarios: The pressure and propulsion energy stored may be suddenly released in case of a structural failure. Hypervelocity impacts of space debris particles are one possible source of tank failures.

In order to reduce the likelihood of tank explosions, ESA's space debris mitigation policy requires the depressurization of the tanks for the disposal phase after the end of the spacecraft operational life. However, the critical pressure level has not yet been sufficiently researched to allow for defining reasonable tank design features or operational measures for disposal. The "Impact-Safe Tank Pressure Level" ("ImSafT") study initiated by ESA and performed by Fraunhofer EMI together with PEAK Technology aims to investigate the effects of impact induced tank failures and derive the critical threshold conditions for catastrophic tank explosions.

There are three main physical effects on a tank's wall upon particle impact: First, the contained fluid exerts a (mostly) static pressure onto the tank wall, which induces tensile stresses in the wall. This pressure varies somewhat, but on a comparatively long time scale (seconds or longer). Static pressure variations occur mainly during the operations phase, but can also occur after end of life (EOL), since spacecraft are usually no longer stabilized and temperature controlled after EOL. E. g. the passage of the solar terminator can cause temperature variations which can result in varying tank pressures.

The second main effect is direct loading of the tank wall by impacting particles. This includes the stress waves generated by the primary impact event into the tank wall [8]. At hypervelocity, both the impacting particle and the tank wall close to the impact location are broken into fragments, including melt, vaporization and ionization. Those fragments are decelerated when travelling through the fluid [3, 10]. Therefore, fragments propagating through the tank may or may not impact the tank's rear wall from inside.

The third main effect comprises wall stresses induced by stress waves generated inside the fluid as a consequence of the impact. Prominent examples for such effects are hydraulic ram [14] and propellant detonation [1, 2, 5] induced stress waves.

2. APPROACH

Investigating tank rupture behaviour resulting from a hypervelocity impact is challenging: When conducting experiments, high procurement and manufacturing costs for representative tank hardware significantly limit the count of hypervelocity impact experiments. With respect to numerical simulations, the combination of large tank volumes (approx. 0.2 to 1 m^3 for realistic on-board tanks) together with the comparatively thin wall thicknesses (in the order of 1 mm) constitutes a significant challenge to establish stable and economically feasible simulations.

*Corresponding author, e-mail robin.putzar@emi.fraunhofer.de, ORCID 0000-0002-1377-0763

Proc. 9th European Conference on Space Debris, Bonn, Germany, 1–4 April 2025, published by the ESA Space Debris Office
Editors: S. Lemmens, T. Flohrer & F. Schmitz, (http://conference.sdo.esoc.esa.int, April 2025)

In the ImSafT study, only a small number of hypervelocity impact tests were planned to limit manufacturing costs. Instead, tank rupture is investigated both by numerical and experimental means. The overall approach comprises four steps: 1. Validate the numerical approach and material models using available impact test data. 2. Predict critical impact conditions using numerical simulations. 3. Confirm the predictions by hypervelocity impact experiments on scaled tanks. 4. Perform parametric numerical simulations on tanks having representative sizes.

This approach involves three different tank geometries: validation case tanks (cylindrical tanks having an outer diameter of 150 mm and a length of 348 mm), tanks for the impact experiments (spherical tanks having an outer diameter of 180 mm), and representative tanks for the parametric numerical simulations (spherical tanks having an outer diameter of 600 mm). Figure 1 shows those three tank geometries in comparison.

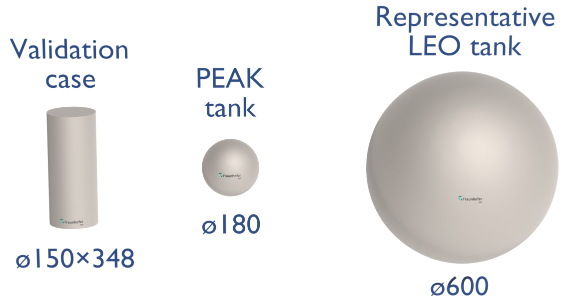

Figure 1. Tank size comparison: The "validation case" tanks (from [11]) were used to validate the numerical approach. The "PEAK tanks" were used in the hypervelocity impact experiments. The "representative LEO tanks" were used in the parametric numerical simulations.

3. VALIDATION OF SIMULATIONS

3.1. Validation cases

As validation case, two tests performed in a previous hypervelocity impact test campaign were selected. The two selected tests are experiment numbers 8385 and 8389 out of a series of ten tests on cylindrical titanium pressure vessels directly impacted by aluminium spheres. The tests were performed at Fraunhofer EMI in frame of an ESA contract and are well documented in a corresponding technical note [9]. The results are also available in public literature [11]. There, they are denoted as tests "Ti-5" (no. 8385) and "Ti-8" (no. 8389). Table 1 lists the tests on titanium pressure vessels from this study.

Experiment no. 8385 resulted in a single perforation hole in the tank's front side, but no perforation at the tank's rear side and no catastrophic rupture. Experiment no. 8389 resulted in catastrophic rupture of the tank, initiated from the rear side. Figures 2 and 3 show photos of the tanks after test.

3.2. General considerations for simulation

The validation simulations were initially performed using Ansys Autodyn. A combined modelling approach using both a Eulerian grid for the fluid and Lagrangian finite elements (FE) for the tank is considered most useful to investigate the (global) pressure wave effects in the tank wall material.

The interaction of the projectile fragments with the (high pressure) gas, leading to fragment deceleration and shock wave formation, works only for Lagrangian FE parts and/or Eulerian multi-material parts. However, the fragmentation for FE parts goes along with the erosion of elements that are replaced by "eroded nodes" [6]. In Autodyn, these eroded nodes do interact with other FE parts, but not with the gas in the Eulerian domain. As a consequence, the eroded nodes are neither decelerated, nor do they contribute to the formation of the (strong) pressure wave. Due to the lack of deceleration, they hit the rear tank wall with an unrealistically high momentum, causing highly localized loads (confined to many small spots). When instead the eroded nodes (i. e. fragments) were interacting with the gas, they would decelerate and amplify the pressure wave inside the gas. This would cause a more extended, more planar load to the rear wall, since the momentum introduced by the projectile is distributed over a larger area. The tank wall resistance against highly localized loads is significantly smaller than to similar loads being more outspread, resulting in a too early failure without interaction between eroded nodes and gas. For realistic simulation results, the projectile therefore needs to be modelled in the Eulerian domain to ensure its interaction with the pressurized gas after fragmentation.

The interaction of the high-pressure gas (Eulerian domain) with the vessel walls (Lagrangian domain) works only properly if an adequate (Eulerian) grid resolution is chosen: The grid size of the Eulerian mesh has to be smaller than the thinnest Lagrangian dimension (1 mm here). This is on the expense of the computation time. Resolving the fragmentation of the projectile was not chosen as a driver for the grid resolution in order to have an acceptable computation time. Generally, the modelling of the fragmentation process of a (small) projectile is, today, still not solved satisfactorily, as the process generates a multi-scale problem. Therefore, the computation time dictates the (minimum) grid resolution. As the selected test cases have two symmetry planes (to take with a grain of salt), we make use of them in order to optimize the computation time versus the level of spatial resolution.

Table 1. *Tests on titanium pressure vessels (Table 14 from Ref. [9]).*

Vessel type	t	EMI No.	d	v	α	E_{kin}	p	σ_H	Damage	
	[mm]		[mm]	[km/s]	[°]	[kJ]	[bar]	[MPa]	cat. burst [type*]	dam. class
Ti 99.6%,1:1	1.02	3202	4.93	6.9	0	4.02	30.3	223	no	A2
Ti 99.6%,1:1	1.02	3207	4.93	6.8	0	3.91	56.0	412	no	A2
Ti 99.6%,1:1	1.02	3224	5.96	6.6	0	6.51	61.4	451	no	B2
Ti 99.6%,1:1	1.02	3229	7.0	6.1	0	9.02	50.6	372	no	B2
Ti 99.6%,1:1	1.02	8385	8.0	7.5	0	21.9	$\approx 16^{\S}$	118	no	B2
Ti 99.6%,1:1	1.02	8384	8.0	7.0	0	19.1	30.2	222	yes [r.s.]	C5
Ti 99.6%,1:1	1.02	8293	8.0	7.0	0	18.1	54.4	400	yes [f.s.]	B4
Ti 99.6%,1:1	1.02	8389	8.9	7.1	0	26.0	23.4	172	yes [r.s.]	C4
Ti 99.6%,1:1	1.02	8386	10.0	7.0	0	36.0	9.3	68	yes [r.s.]	C4
Ti 99.6%,1:1	1.02	8292	10.0	6.8	0	33.5	55.7	410	yes [r.s.]	C5

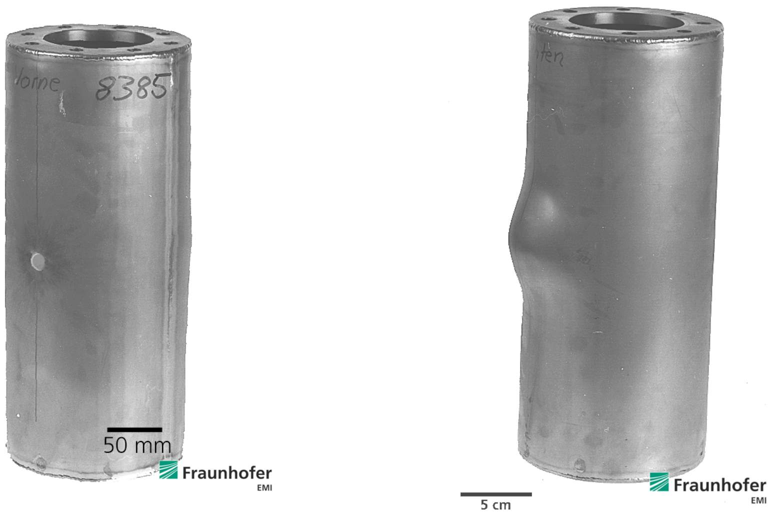

Figure 2. Result from test 8385. Left: front side, right: rear side. © Fraunhofer EMI.

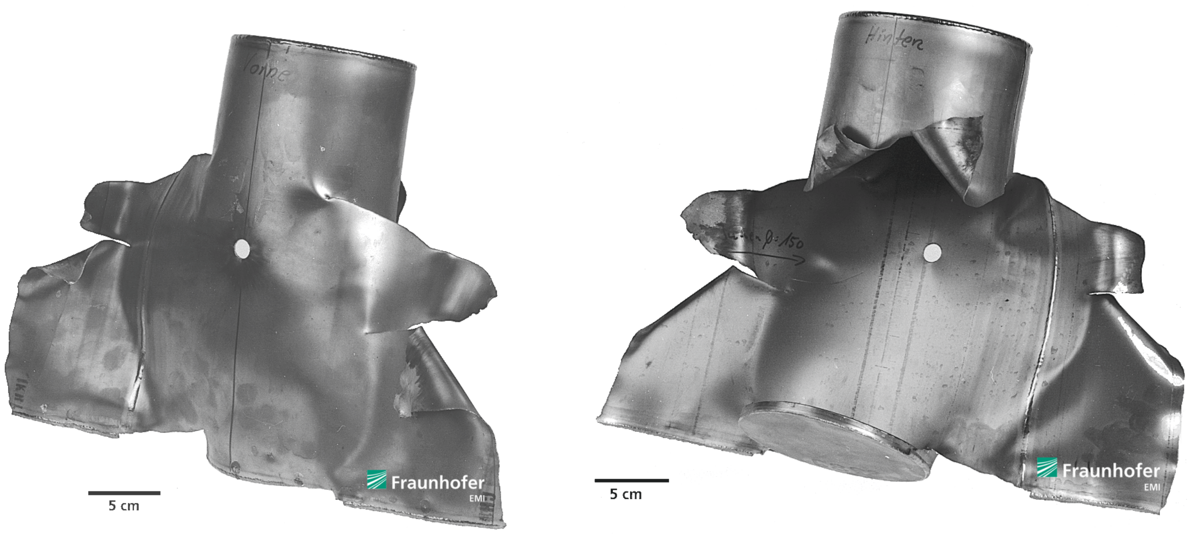

Figure 3. Result from test 8389. Left: front side, right: rear side. © Fraunhofer EMI.

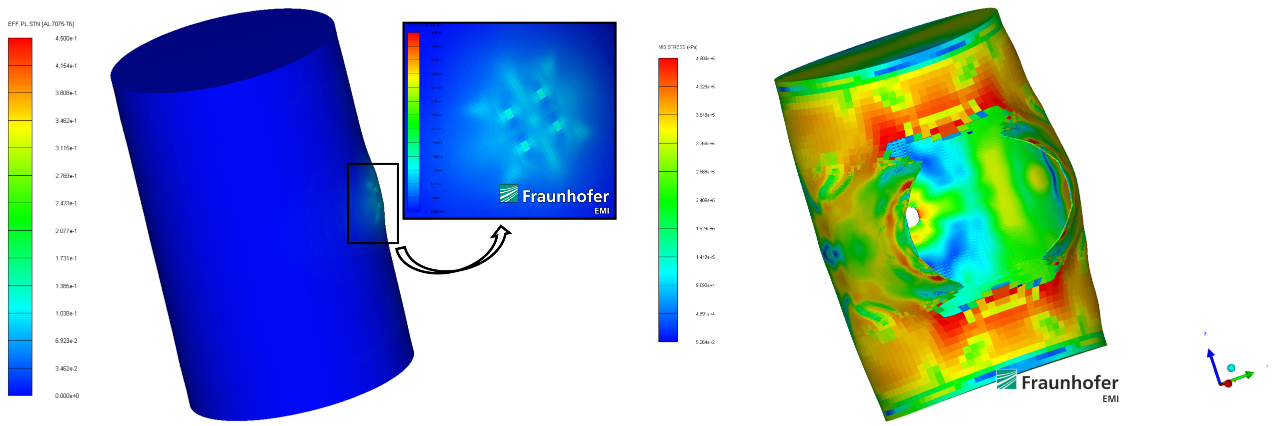

Figure 4. Simulation snapshots from Autodyn. Left: Effective plastic strain after 1 ms in simulated test 8385. Right: von Mises equivalent stress distribution after 780 µs in simulated test 8389. © Fraunhofer EMI.

3.3. Autodyn results

Despite initial issues, the simulations of the validation cases using Autodyn could be completed successfully. In the simulations, the tanks were filled with nitrogen gas to the pressure which was present in the test, and subsequently impacted by an aluminium sphere projectile. Figure 4 shows some results. The comparison illustrates the good qualitative accordance between simulation and test with respect to the threshold criteria. For the non-catastrophic case, we only observe a bulging at the backside of the vessel with maximal values of effective plastic strain well below the limit used in the material failure description. With the same material data, including the failure criterion, we observe a catastrophic burst in the simulation that corresponds well to the catastrophic burst in the respective test.

It is noted that the result of the experiment 8385 is at the very limit to a catastrophic burst. Therefore, we have chosen to simulate an impact with a clear (assumed) distance to this threshold by reducing the impact energy in terms of impact velocity (7.0 km/s instead of 7.5 km/s) and projectile size (7.0 mm instead of 8.0 mm).

The next step involved applying the same method to the other two tank sizes investigated in the study, i.e. the 180 mm diameter PEAK tank and the 600 mm diameter representative LEO tank, cf. figure 1. However, the simulations became unstable for different tank sizes. Despite a significant effort, which also involved varying the material parameters for different tank sizes, no stable numerical set-up for all tank sizes could be established with Autodyn. In a next step, simulations in LS-Dyna were tried, but the result was the same.

In summary, both commercial tools Ansys Autodyn and LS-Dyna showed critical stability issues for the large-scale tank simulations. We investigated various mechanisms for the fluid-solid-coupling and meshing. Despite more than 120 simulations performed, our own expertise with the tools and intensive exchange with the support service of the commercial tools, no solution could be found.

3.4. SOPHIA-APOLLO coupling

Finally it was decided to further develop the coupling between the two in-house tools SOPHIA (a computational structural dynamics tool) and APOLLO (a computational fluid dynamics tool) to solve the described numerical issues.

The impact simulation on the Lagrangian structure side of tank and projectile is carried out with the SOPHIA code. After material failure of tank or projectile elements, eroded elements are converted into SPH particles. An empirical model [10] is used to calculate the diameter and number of the particles resulting from the impact, and the properties of the resulting particles are exchanged with APOLLO.

The shock wave propagation in the fluid is simulated by the APOLLO Blastsimulator, which was developed especially for detonation processes and shock wave propagation. Efficiency and accuracy of the APOLLO Blastsimulator rely on dynamic mesh adaption: the domain size is automatically adapted to the global extent of the flow, and the mesh resolution is automatically adapted to local flow features such as shock fronts and material interfaces. Thereby, the computational effort is spent only on relevant regions of the flow field. The properties of the fluid acting on the Lagrangian structures, including the eroded SPH particles, are transferred back to SOPHIA.

3.5. SOPHIA-APOLLO results

Since the numerical method was changed, the validation cases needed re-evaluation. All ten experiments listed in table 1 were simulated. The validation case tanks were simulated in a full three-dimensional model without symmetries. In the simulations, a cylinder made of titanium with an outer diameter of 150 mm, a somewhat reduced height of 212 mm (to expedite simulation time) and a wall thickness of 1 mm is modelled. The element size for the vessel is between 0.3 and 5 mm, resulting in ca. 160 000 elements. The projectile is aluminium with diameters between 4.93 and 10 mm and initial impact velocities between 5 and 8 km/s. The element size for the projectile is between 0.3 to 1 mm, resulting in ca. 3 600 elements.

The fluid was modelled via APOLLO, with an ambient pressure of 1 bar outside the vessel and filled inside the vessel with an ideal gas with pressure according to table 1. The Eulerian grid resolution is 16 mm (zonal length of the basic grid) with a level 4 refinement (factor 16) which results in a minimal grid size of 1 mm. The dimensions of the fluid domain are 0.24, 0.22 and 0.3 m³ for the x, y and z directions, respectively, with ca. 3900 grid cells of the basic grid and ca. 158 million grid cells at the highest resolution.

A comparison of the simulations with the experiments showed that the structural failure of the rear side of the tank is consistent with the existing experiments and the empirical prediction. There also were discrepancies in some simulations with respect to front side bursting of the vessels. Overall, the fluid-structure coupling of APOLLO and SOPHIA was found to be suitable for mapping a high-speed impact on a pressurized tank structure. Figures 5 to 8 show the results for the two chosen test cases, experiments 8385 and 8389.

Figure 5. Simulation with SOPHIA-APOLLO of test 8385: Vessel deformation from the front (left) and rear (right) side at the end of the simulation at 0.5 ms. © Fraunhofer EMI.

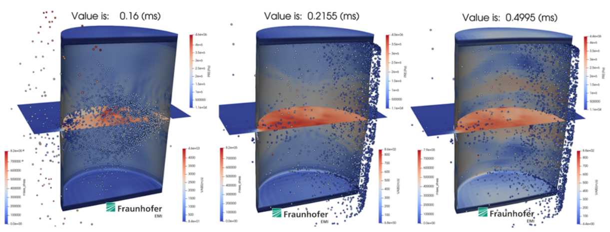

Figure 6. Simulation with SOPHIA-APOLLO of test 8385: Snapshots of the von Mises stress in the tank hull, fluid pressure and particle velocity at different time steps. © Fraunhofer EMI.

Figure 7. Simulation with SOPHIA-APOLLO of test 8389: Vessel deformation from the front (left) and rear (right) side at the end of the simulation at 0.5 ms. © Fraunhofer EMI.

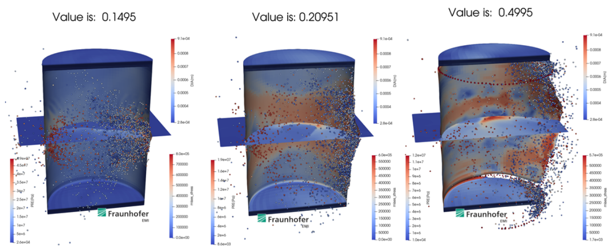

Figure 8. Simulation with SOPHIA-APOLLO of test 8389: Snapshots of the von Mises stress in the tank hull, fluid pressure and particle velocity at different time steps. © Fraunhofer EMI.

3.6. Material Parameter

Numerical simulations require validated material data. The three tank types investigated in the study (figure 1) are composed of two different titanium alloy materials. The PEAK tanks were made of 3.7035, which is also known as titanium ASTM grade 2 (Ti-2). The validation case tanks were made of Tikrutan RT 15, which is considered equivalent to Ti-2 [4]. The representative LEO tanks are made of 3.7165, also known as Ti-6Al-4V or titanium ASTM grade 5.

The publicly available material data for those two alloys is limited, especially at high strain rates. Therefore, a material characterization campaign was performed at Fraunhofer EMI, which included tensile tests at 0.001 /s and 1000 /s, reverse Taylor impact tests and planar plate impact tests. All those tests were performed on the same material batch of Ti-2, which was used to manufacture the PEAK tanks. Those tests and their results are subject to a dedicated publication, therefore not further reported here.

4. TANK MANUFACTURING

For the hypervelocity impact tests, spherical titanium tanks were manufactured by PEAK Technology GmbH, Austria. 180 mm were chosen as the outer diameter of the tanks, mainly to keep manufacturing costs at a reasonable level.

This is considerably smaller than representative tanks, cf. section 2 and figure 1. According to Barlow's formula (1) (given here for spheres), a reduction of the tank diameter results in an increased burst pressure p when maintaining all other parameters (here: maximum tolerable wall stress σ, internal tank diameter d and tank wall thickness t):

$$\sigma = \frac{p \cdot d}{4 \cdot t} \quad \Leftrightarrow \quad p = \frac{4 \cdot \sigma \cdot t}{d} \tag{1}$$

Facility-wise, the tank fill pressure was limited to 10 MPa (100 bar). Since tests at the very limit of the tank loading capacity were planned, the tank burst pressure was effectively limited to 10 MPa. To achieve this limit, both the wall thickness and the tensile strength of the wall material were reduced. Effectively, the maximum diameter and the maximum burst pressure were the two most important parameters for the design of the tanks to be subjected to hypervelocity impact tests.

Materials under review were Ti-2 and Ti-6Al-4V. Only one material could be used to stay within the available budget for sample manufacturing in terms of engineering models and welding probes. Because the minimum wall thickness is also limited by manufacturing constraints, the weaker material Ti-2 was chosen. The yield stress of Ti-6Al-4V is around 830 MPa, for the Ti-2 used it is at 312.7 MPa.

Tanks with two different wall thicknesses were manufactured: 0.6 mm and 0.9 mm. Each tank was manufactured from two identical hemispherical endcaps, which were welded together. Each tank is plane symmetric through its equator (weld), meaning that both ends of the tank are open and provide the same interface.

A total number of ten tanks were manufactured, five tanks per wall thickness. Four tanks of each wall thickness were used for the impact tests, whereas the remaining two tanks were subjected to burst pressure testing.

4.1. Burst pressure testing

The burst pressure p was estimated before manufacturing using Barlow's formula for spheres (1). When the tank is inflated, the internal pressure imposes stresses in circumferential direction. These stresses cause strain, which is equivalent to an increase of the tank diameter. To account for this diameter change, the corresponding strain is calculated assuming linear elastic behaviour:

$$\sigma = E \cdot \varepsilon \quad \Rightarrow \quad \Delta d = \varepsilon \cdot d = \frac{\sigma \cdot d}{E} \tag{2}$$

with diameter increase Δd, strain ε and elastic modulus E. This approach is considered conservative, as the increased diameter results in a lower calculated burst pressure.

From equation (2), the diameter increase calculates to $\Delta d \approx 0.844$ mm from $E = 103$ GPa, the ultimate tensile strength $\sigma = 483$ MPa and the original tank diameter $d = 180$ mm. Using equation (1) and a diameter $d = 180.84$ mm, the burst pressure calculates to $p \approx 6.41$ MPa $= 64.1$ bar for the tanks with $t = 0.6$ mm wall thickness and to $p \approx 9.61$ MPa $= 96.1$ bar for the tanks with $t = 0.9$ mm wall thickness.

To verify the results, one tank of each wall thickness was pressurized until its ultimate burst. The tank was filled with water, and the internal pressure was increased at a rate of 0.1 MPa/s $= 1$ bar/s until failure. Distilled water was used as pressurant. Figure 9 illustrates the set-up for the burst test. In this figure, arrow 1 indicates the water inlet from the pump, arrow 2 indicates the pressure sensor controlling the pump and arrow 3 indicates the pressure sensor used for logging the internal pressure.

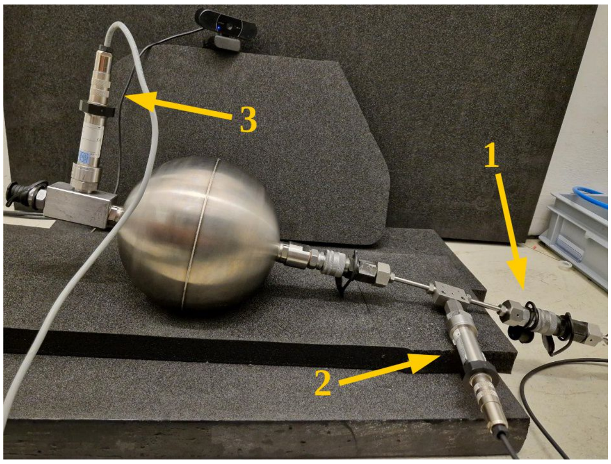

Figure 9. Burst test set-up. 1 – water inlet, 2 – pressure sensor controlling the pump, 3 – pressure sensor for logging. © Peak Technology GmbH.

Figures 10 and 11 show the two tank samples after the burst tests. The measured burst pressure values were 7.73 MPa for the tank with 0.6 mm wall thickness and 11.05 MPa for the tank with 0.9 mm wall thickness.

To identify possible explanations for the discrepancy between predicted and measured burst pressures, Barlow's formula (1) was re-evaluated taking into account the actual ultimate tensile stress of the material (the maximum true stress value measured in quasistatic testing at Fraunhofer EMI, cf. section 3.6, which is 703.9 MPa), the measured tank wall thickness after burst in the burst region (0.52 mm and 0.75 mm for 0.6 mm and 0.9 mm nominal wall thickness, respectively), and the approximate inner diameter of the tank before burst (190.70 mm and 196.95 mm for 0.6 mm and 0.9 mm nominal wall thickness, respectively). The results of the re-calculations are given in Table 2. Overall, the re-evaluated burst pressures are in good agreement with the measured values.

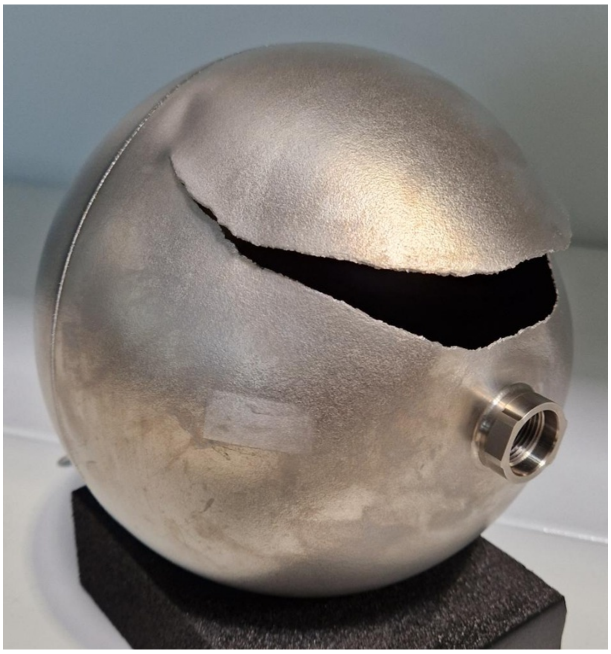

Figure 10. Tank sample with 0.9 mm wall thickness after burst test. © Peak Technology GmbH.

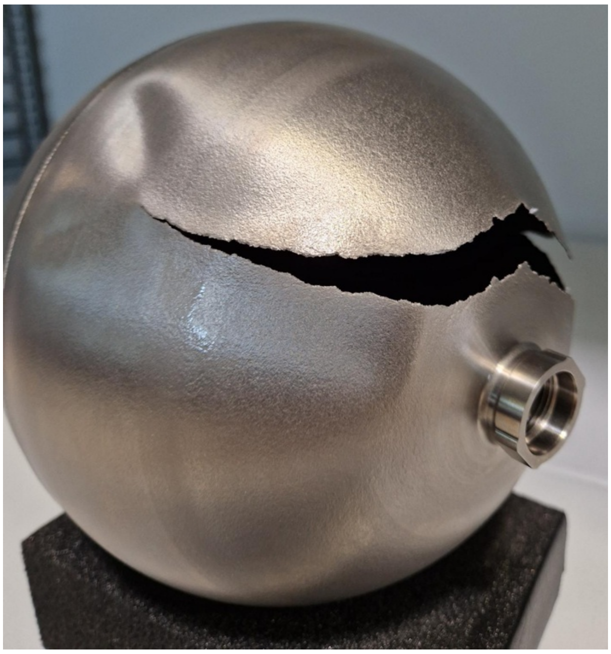

Figure 11. Tank sample with 0.6 mm wall thickness after burst test. © Peak Technology GmbH.

Table 2. Predicted, measured, and re-evaluated tank burst pressures for the two wall thicknesses.

Nominal wall thickness	0.6 mm	0.9 mm
Predicted burst pressure	6.41 MPa	9.62 MPa
Measured burst pressure	7.73 MPa	11.05 MPa
Re-evaluated burst pressure	7.68 MPa	10.72 MPa
Measurement count	1	1

5. HYPERVELOCITY IMPACT TESTING

Eight hypervelocity impact tests were performed at Fraunhofer EMI's Space Gun facility. The tanks were placed into the target chamber, filled with dry nitrogen gas and impacted directly, i. e. with no additional shielding. Figure 12 shows an example photograph of a tank target inside the target chamber prior impact testing. Figure 12 also indicates the locations of the pressure sensor, the pressure feed and the shot axis.

The tank placement differed for impact tests at 0° and 45° impact angle. Figure 13 shows a sketch of the tank location for both impact angles.

Projectiles were spheres made of pure aluminum. 7.5 and 8.0 mm diameter spheres were used as impactors.

5.1. Test matrix

Table 3 lists all impact tests performed.

Tests 6548 and 6578 did not quite run as expected:

1. In test 6548, a small sabot piece impacted the tank ca. 5 µs after the projectile at approximately the same velocity. The estimated mass of this piece is 10 to 20 mg, in any case less than 50 mg. resulting in an additional impact energy of ca. 150 to 300 J. The target fragments retrieved after the test show that the sabot piece impacted very close to the projectile. The effect of the sabot impact is considered negligible.

2. In test 6578, the laser light barrier projectile velocity measurement system was not operating correctly. The velocity was measured through muzzle and impact flash. This measurement is coarser, therefore the velocity accuracy is not as high as with the other experiments. Also, no high-speed videos were recorded during this test.

5.2. Mechanical damage

In the three tests 6548, 6576 and 6578, the tank ruptured. In tests 6548 and 6578, the rupture initiated from the tank's front side. In test 6576, the rupture initiated from the tank's rear side.

In tests 6547 and 6577, the projectile fragments did not perforate the rear side of the tank. The tank rear side shows some impact craters. In test 6577, the rear side also shows some bulges, which are not present in test 6547.

In tests 6552, 6553 and 6554, the projectile fragments perforated the tank's rear side. The overall energy, however, was not sufficient to cause rupture.

Figures 14 to 17 show photos of the rear side damage of the tests 6547, 6577, 6553 and 6554.

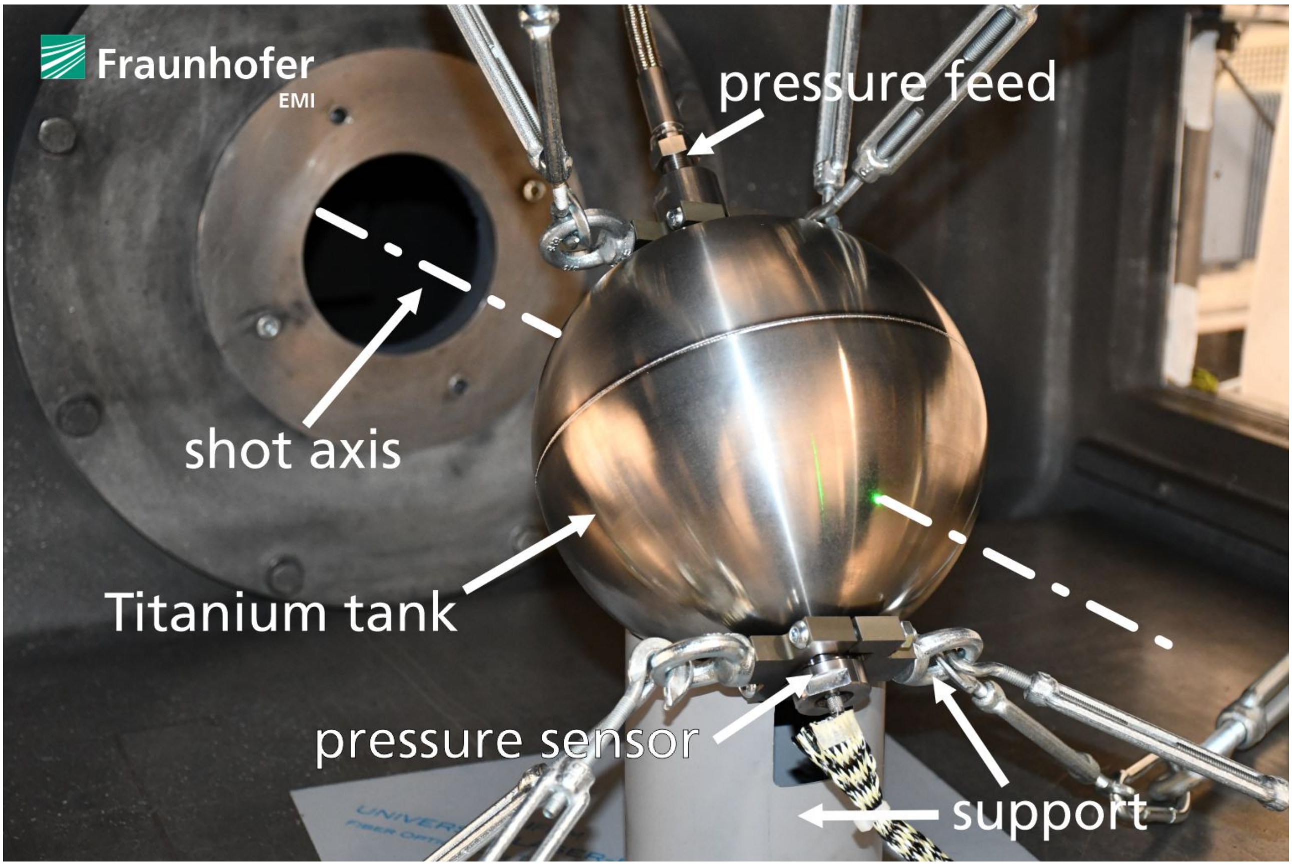

Figure 12. Photo of titanium tank sample in target chamber prior impact testing (exp. 6547). © Fraunhofer EMI.

Table 3. Hypervelocity impact tests performed. t – nominal tank wall thickness, p – inner tank pressure, θ – impact angle, d_P – nominal projectile diameter, m_P – measured projectile mass, v – impact velocity, E – projectile kinetic energy at impact, Comments – see text in section 5.1.

No.	t [mm]	p [MPa]	θ [°]	d_P [mm]	m_P [mg]	v [km/s]	E [J]	Test result	Comments
6547	0.9	7.2	0	7.5	598.3	5.39±0.02	8.68±0.05	no burst	
6548	0.9	7.2	0	8.0	728.0	5.39±0.02	10.58±0.06	burst, front	1.
6577	0.9	7.2	45	7.5	599.8	5.45±0.02	8.91±0.05	no burst	
6578	0.9	7.2	45	8.0	726.8	5.19±0.10	9.79±0.38	burst, front	2.
6552	0.6	1.2	0	8.0	724.5	5.15±0.02	9.62±0.06	no burst	
6553	0.6	1.6	0	8.0	725.5	5.01±0.02	9.09±0.06	no burst	
6554	0.6	2.0	0	8.0	727.3	5.35±0.02	10.40±0.06	no burst	
6576	0.6	2.6	0	8.0	726.6	5.30±0.02	10.32±0.06	burst, rear	

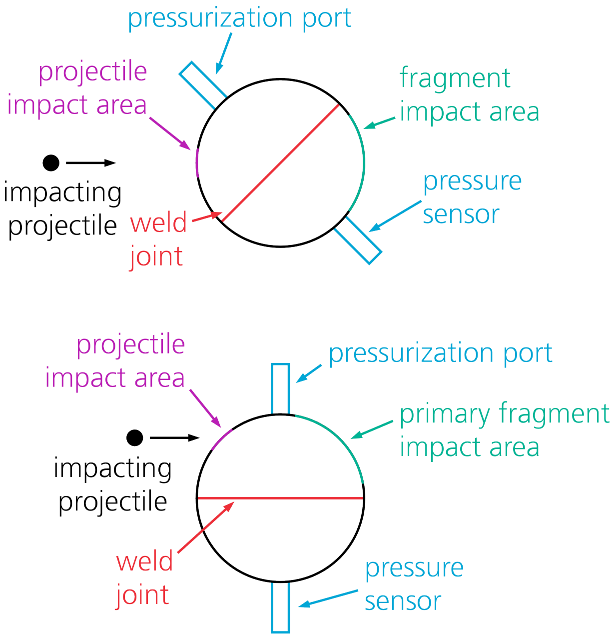

Figure 13. Tank placement for 0° (top) and 45° (bottom) impact tests. © Fraunhofer EMI.

Figure 14. Rear side of tank after test 6547 with no visible damage. © Fraunhofer EMI.

5.3. Rupture behaviour

The tests indicate that the rupture of tanks has three prerequisites: a location where the tank wall is perforated, sufficient internal pressure, and a pressure pulse acting on the tank wall from the inside which is generated by the fragment cloud moving through the gas.

The perforation seems to act as a nucleus (starting point) for cracks. Once cracks have started to form, their growth seems to be driven by a combination of the pressure pulse generated by the projectile's fragments and the pressure difference between the inside and the outside of the tank.

Tests 6553, 6554 and 6576 show that there is an influence of the pressure difference on the mechanical damage to the tank. In test 6553 with 16 bar pressure difference, the cracks expanded to a hole having a size of 43 × 46 mm (horizontal × vertical). In test 6554 with 20 bar pressure difference, the cracks expanded to a significantly larger hole having a size of 74 × 76 mm. In test 6576 with 26 bar pressure difference, the tank ruptured.

In all experiments with 0.9 mm wall thickness, the internal pressure was significantly higher than in the experiments with 0.6 mm wall thickness. Due to this higher pressure, the projectile fragments were significantly decelerated within the nitrogen gas and could not cause perforation of the rear side. This was true for both the 0° tests, where the fragments were required to travel the entire diameter, as well as for the 45° tests, where the fragments were only required to travel half a diameter due to the different impact location.

Figure 15. Rear side of tank after test 6577 with visible bulges. © Fraunhofer EMI.

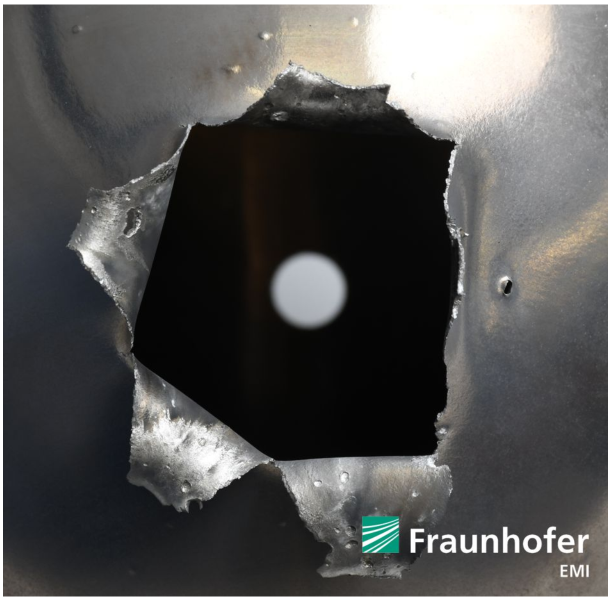

Figure 16. Rear hole in tank after test 6553. The hole size is 43 × 46 mm (horizontal × vertical). The front hole diameter is 11.7 mm. © Fraunhofer EMI.

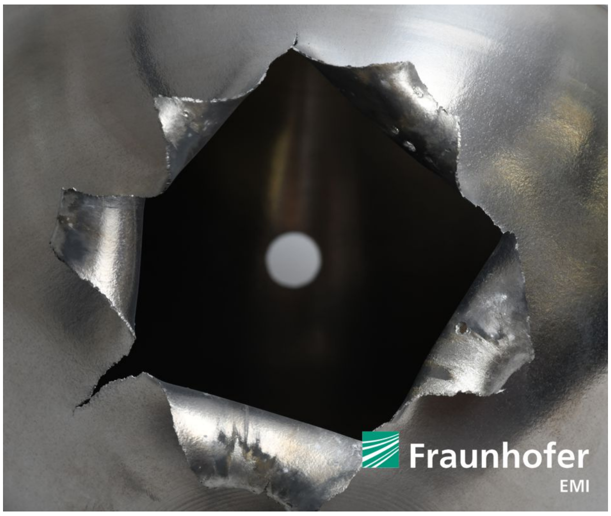

Figure 17. Rear hole in tank after test 6554. The hole size is 74 × 76 mm (horizontal × vertical). The front hole diameter is 12.2 mm. © Fraunhofer EMI.

6. CONCLUDING REMARKS

Investigating tank rupture caused by hypervelocity impact is challenging. On the experimental side, comparatively high manufacturing costs make large-scale impact testing expensive. On the numerical side, the combination of large tank volumes and small wall thicknesses pose a significant challenge for available solvers.

The numerical simulations and hypervelocity impact tests conducted at Fraunhofer EMI's Space Gun facility once more showed the complex interaction between the fragments generated upon perforation of the first tank wall and the pressurized gas inside the tank. This raises the question on the accuracy of models which employ a single curve for both front and rear side bursting like the one published by Schonberg [12, 13].

The parametric numerical study is currently in progress.

ACKNOWLEDGMENT

The work presented herein was carried out under a programme of, and funded by, the European Space Agency under ESA contract 4000126122/18/NL/LvH. The view expressed in this publications can in no way be taken to reflect the official opinion of the European Space Agency.

ACRONYMS

EMI	Fraunhofer Ernst-Mach-Institut
EOL	end of life
ESA	European Space Agency
FE	finite element
ImSafT	Impact-Safe Tank Pressure Level
SPH	smoothed-particle hydrodynamics
Ti-2	3.7035, or titanium ASTM grade 2

AI USE

No artificial intelligence tools were used by the authors to produce or modify any part of this manuscript.

REFERENCES

[1] H. Abdulhamid, P. Deconinck, F. Pacaud, and J. Mespoulet. "Explosiveness conditions of hydrazine under HVI : Part 2 : Results". In: *71st Meeting of the Aeroballistic Range Association*. 2022.

[2] H. Abdulhamid, P. Deconinck, F. Pacaud, and J. Mespoulet. “Explosiveness of hydrazine under high velocity impact : Part 1 : Safety analysis and high speed valve development”. In: *71st Meeting of the Aeroballistic Range Association*. 2022.

[3] S. Hiermaier and F. Schäfer. “Hypervelocity impact fragment clouds in high pressure gas - numerical and experimental investigations”. In: *International Journal of Impact Engineering* 23 (1999), pp. 391–400. DOI: 10.1016/S0734-743X(99)00089-5.

[4] H. Hucek and M. J. Wahll. *Handbook of international alloy compositions and designations, volume I - titanium*. ADA 036433, MCIC-HB-09-VOL-1. Columbus, Ohio, USA: Metals and Ceramics Information Center, 1976. URL: https://apps.dtic.mil/sti/citations/tr/ADA036433.

[5] J. Limido, C. Puillet, and J.-P. Vila. “Explosion of hydrazine tanks due to space debris impacts”. In: *2019 15th Hypervelocity Impact Symposium*. 2019, pp. 589–597. DOI: 10.1115/HVIS2019-099.

[6] P. Matura, G. Heilig, M. Lueck, and M. Sauer. “Simulation and experiments of hypervelocity impact in containers with fluid and granular fillings”. In: *Procedia Engineering* 103 (2015), pp. 365–372. ISSN: 1877-7058. DOI: 10.1016/j.proeng.2015.04.034.

[7] NASA Orbital Debris Program Office. “Monthly number of objects in earth orbit by object type”. In: *Orbital Debris Quarterly News* 29.1 (2025), p. 8. URL: https://orbitaldebris.jsc.nasa.gov/quarterly-news/.

[8] S. Ryan, F. Schäfer, M. Guyot, S. Hiermaier, and M. Lambert. “Characterizing the transient response of CFRP/Al HC spacecraft structures induced by space debris impact at hypervelocity”. In: *International Journal of Impact Engineering* 35.12 (2008), pp. 1756–1763. DOI: 10.1016/j.ijimpeng.2008.07.071.

[9] F. Schäfer. *Hypervelocity impact testing: Impacts on pressure vessels: Final report*. EMI-Bericht I-27/01. Freiburg im Breisgau, Germany: Fraunhofer-Institut für Kurzzeitdynamik, Ernst-Mach-Institut, 2001.

[10] F. Schäfer. “An engineering fragmentation model for the impact of spherical projectiles on thin metallic plates”. In: *International Journal of Impact Engineering* 33 (2006), pp. 745–762. DOI: 10.1016/j.ijimpeng.2006.09.067.

[11] F. Schäfer, E. Schneider, and M. Lambert. “Hypervelocity impacts on cylindrical pressure vessels - experimental results and damage classification”. In: *Pressure Vessels and Piping Conference*. 1997.

[12] W. P. Schonberg. “Meeting passivation requirements for spacecraft pressure vessels and fuel tanks”. In: *Journal of Space Safety Engineering* 7.3 (2020), pp. 222–229. DOI: 10.1016/j.jsse.2020.06.002.

[13] W. P. Schonberg and J. M. Ratliff. “Hypervelocity impact of a pressurized vessel: Comparison of ballistic limit equation predictions with test data and rupture limit equation development”. In: *Acta Astronautica* 115 (2015), pp. 400–406. DOI: 10.1016/j.actaastro.2015.06.013.

[14] D. Townsend, N. Park, and P. M. Devall. “Failure of fluid filled structures due to high velocity fragment impact”. In: *International Journal of Impact Engineering* 29.1 (2003), pp. 723–733. DOI: 10.1016/j.ijimpeng.2003.10.019.